Exponential acceleration of macroscopic quantum tunneling in a Floquet Ising model

```
George Grattan<sup>1,2</sup>, Brandon A. Barton<sup>1,3</sup>, Sean Feeney<sup>1</sup>, Gianni Mossi<sup>5,6</sup>, Pratik Patnaik<sup>1,4</sup>,

Jacob C. Sagal<sup>1</sup>, Lincoln D. Carr<sup>1,3,4</sup>, Vadim Oganesyan<sup>7,8,9</sup>, and Eliot Kapit<sup>1,4*</sup>

<sup>1</sup> Quantum Engineering Program, Colorado School of Mines, 1523 Illinois St, Golden CO 80401

<sup>2</sup> Department of Computer Science, Colorado School of Mines, 1500 Illinois St, Golden CO 80401

<sup>3</sup> Department of Applied Mathematics and Statistics,

Colorado School of Mines, 1500 Illinois St, Golden CO 80401

<sup>4</sup> Department of Physics, Colorado School of Mines, 1523 Illinois St, Golden CO 80401

<sup>5</sup> KBR, Inc., 601 Jefferson St., Houston, TX 77002, USA.

<sup>6</sup> Quantum Artificial Intelligence Lab. (QuAIL),

NASA Ames Research Center, Moffett Field, CA 94035, USA.

<sup>7</sup> Department of Physics and Astronomy, College of Staten Island, CUNY, Staten Island, NY 10314, USA

<sup>8</sup> Physics program and Initiative for the Theoretical Sciences,

The Graduate Center, CUNY, New York, NY 10016, USA and

<sup>9</sup> Center for Computational Quantum Physics, Flatiron Institute, 162 5th Avenue, New York, NY 10010, USA*
```

The exponential suppression of macroscopic quantum tunneling (MQT) in the number of elements to be reconfigured is an essential element of broken symmetry phases. Slow MQT is also a core bottleneck in quantum algorithms, such as traversing an energy landscape in optimization, and adiabatic state preparation more generally. In this work, we demonstrate the possibility to accelerate MQT through Floquet engineering with the application of a uniform, high frequency transverse drive field. Using the ferromagnetic phase of the transverse field Ising model in one and two dimensions as a prototypical example, we identify three qualitatively distinct regimes as a function of drive strength: (i) for weak drive, the system exhibits exponentially slow MQT alongside robust magnetic order, as expected; (ii) at intermediate drive strength, we find polynomial decay of rates alongside vanishing magnetic order consistent with critical or paramagnetic state; (iii) at very strong drive strengths both the tunnelling rate and time-averaged magnetic order are approximately constant with increasing system size. We support these claims with extensive full wavefunction and matrix-product state numerical simulations, and theoretical analysis. An experimental test of these results presents a technologically important and novel scientific question accessible on NISQ-era quantum computers.

The idea of single-particle quantum tunneling through a barrier is well-known since the 1920s [1, 2] and is found in practical technologies such as the tunneling diode [3]. Common examples of macroscopic quantum tunneling (MQT) have typically built on this concept [4], including the Josephson junction, a building block of quantum information systems, and can be modeled by e.g. the Lipkin-Meshkov-Glick model [5]. A long-time goal of such models is to move beyond the Josephson regime, in which N bosons or Cooper pairs move fluidly between two dominant single-particle states a particle at a time, into the Fock regime, in which all particles can collectively tunnel from one extreme to the other – the $|N,0\rangle$ and $|0,N\rangle$ NOON state. This is also called the Fock regime, and is produced by raising the effective barrier between these two extremes. This kind of tunneling is hard to observe because the tunneling time is exponentially long in the number of particles. One way to understand this exponentially long time is to calculate the energy splitting between symmetric and anti-symmetric states $|N,0\rangle \pm |0,N\rangle$, which is exponentially small in the Fock regime. The tunneling time can be estimated as hbar over this energy splitting. Such concepts are the basis of symmetry breaking and are famously cited in Anderson's paper, "More is Different" [6], where he uses the example of left and right handed sugar as the two extremes. In this case, the tunneling time is longer than the lifetime of the universe. However, the current quantum computing paradigm and NISQ device availability offer a new opportunity to rexamine such foundational questions, due to their high level of many-body control in both time and space. Utilizing many-body control in the form of symphonic tunneling [7] on the transverse field Ising model (TFIM), in this Letter we establish a complexity transition in MQT from exponential suppression to a polynomial scaling in the number of particles.

Prior to the wide availability of NISQ quantum computing devices and the spread of the quantum circuit paradigm, many researchers looked for ways to observe MQT, such as scattering solitons or "lumps" of bosons on a barrier [8], physically manipulating complicated traps in quantum simulator experiments [9, 10], hybridizing modes to access new avenues for quantum control [11, 12], or driving non- or weakly-interacting systems [13, 14]. A particularly famous example is the beam splitter experiment of Markus Arndt [15], in which fullerenes take two simultaneous paths. Although these experiments are in a certain sense macroscopic [16], ultimately they are mean-field like superpositions of center of mass degrees of freedom [4], just like Josephson tunneling.

However, no one to date has determined a realistic way to achieve MQT of large numbers of strongly-interacting

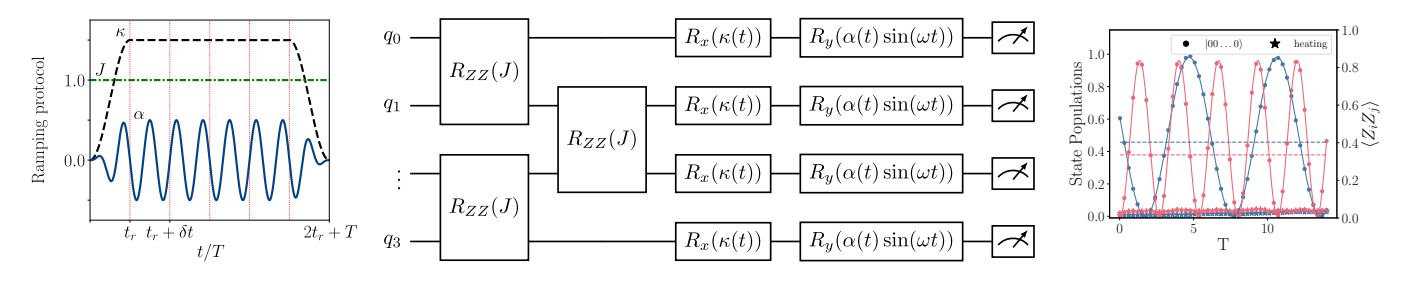


FIG. 1: Adiabatic ramping protocols in (a) for the coefficients $\{J, \kappa, \alpha\}$ in Eq. (1). Both the X (DC) and Y (AC) fields are smoothly ramped up from $0 \to t_r$ and down from $(t_r + T) \to (2t_r + T)$ with the same sinusoidal profile. The circuit in (b) is repeated with varying plateau times T to measure the period of ocscillation. Time traces (c) used to extract the oscillation period Ω_R , for a 4×7 2d geometry, with $\kappa = 2.5$ and two choices of α/f . We plot the final population of $|00...0\rangle$ (after ramping fields down), for a series of plateau times T. The average ferromagnetic correlator $\langle Z_i Z_j \rangle$ (dashed lines) is measured repeatedly during evolution for drive strengths $\alpha/f = 0.1$ (blue) and 0.14 (red) with sinusoidal fits (solid curves) and an estimate of heating $1 - |\langle \psi_f | 00...0 \rangle|^2 - |\langle \psi_f | 11...1 \rangle|^2$ (stars near zero).

quantum elements in a Fock-like regime, and even controlling small numbers of weakly interacting fermions has been a grand challenge only recently accomplished in microtraps [17]. This is a desirable goal in order to traverse energy landscapes, for instance, to find a ground state of a spin glass [18, 19]. MQT physics forms a key source of potential quantum advantage, and bottleneck process for quantum optimization [20, 21]. While we have previously explored multi-tone drives to accelerate MQT scaling[7, 22, 23], in this work we focus on a single frequency Floquet engineering approach [24], which we implement via Trotterization[25] in discrete space-time, i.e. on a quantum circuit model in one and two dimensional lattices of qubits. In addition to the expected ferromagnetic and crossover (critical or paramagnetic) behaviors observed at weak and intermediate drives, we discover an unusual revival of ferromagnetic order at very strong drives accompanied by comparatively fast MQT. The Floquet TFIM we study is

$$H = -J\sum_{\langle ij\rangle} Z_i Z_j - \kappa \sum_i X_i + \alpha \sin \omega t \sum_i Y_i, \qquad (1)$$

here J denotes spin-spin interaction that favors a double degenerate ferromagnetic (FM) ground state (GS), κ is the transverse field, the last term is a uniform field with amplitude and frequency chosen appropriately (see below). The phase transition to a paramagnetic state occurs (for $\alpha=0$) at $\kappa_c=\kappa/J=1$ (\simeq 3) in 1d (2d) [26]. For $\kappa<\kappa_c$, the ground state manifold is a doublet of symmetric and antisymmetric superpositions of macroscopic polarization states with energy splitting $\Omega_0\left(N\right)$, often referred to as a Rabi frequency given the simplicity of the two-level dynamics that ensues. This splitting $\Omega_0\left(N\right)$ —the inverse of which sets the MQT time to mix the two ferromagnetic states—decays exponentially in N. In particular, in 1d, (see Supp. Materials (SM))

$$\Omega_0(N) \propto \frac{\kappa}{\sqrt{N}} \left(\frac{\kappa}{J}\right)^{N-1}.$$
 (2)

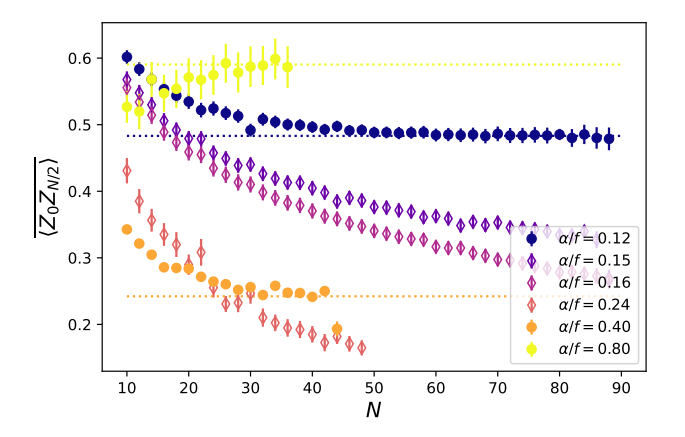
The analogous expression in 2d is expected to be much more complicated, but still scales exponentially in N, i.e. area-like.

To measure the tunneling rate we initialize the system (Fig. 1, left) in one of the FM groundstates of the TFIM for $\kappa = \alpha = 0$, and smoothly ramp up off-diagonal terms κ and α . This creates a coherent magnetization reversal (Rabi) oscillation which we measure by varying the duration of the plateau and fitting the probability of magnetization reversal after ramping down to a simple cosine profile (Fig. 1, right). Magnetic order is inferred from the time average of the two-point correlation $\langle Z_i Z_j \rangle$ over the entire plateau region evaluated at large spatial separations. Our Trotterized simulations closely model how a gate-based quantum computer would approximate the continuum time evolution of the problem (Fig. 1, center), i.e. with a sufficiently small time step (see SM).

The presence of sufficiently strong AC drive in Eq. 1 is expected to induce several new multispin terms in the effective Floquet Hamiltonian of the problem (see SM) steering coherent and/or correlated many-body behavior using such dynamically generated Hamiltonians is commonly referred to as Floquet engineering. Specifically, this work demonstrates the apparent dramatic renormalization of Rabi frequency and magnetic order upon increasing α . However, we must first address the issue of heating, as it is expected to be present in any driven many-body problem. To mitigate it we implement a scaling limit in which the drive frequency and amplitude both increase logarithmically with N. This choice is motivated by the expectation that heating rates from highfrequency drives decay exponentially in ω [27–33], but increase only quadratically with drive amplitude [28]. We thus redefine the Floquet controls as α , f with

$$\alpha \equiv \alpha_s \log N, \ \omega = 2\pi f \equiv 2\pi f_s \log N$$
 (3)

such that the state evolves as $|\psi(t+dt)\rangle = \exp(-2\pi i dt H(t)) |\psi(t)\rangle$. The corrections to the Floquet Hamiltonian are generated as a power series in



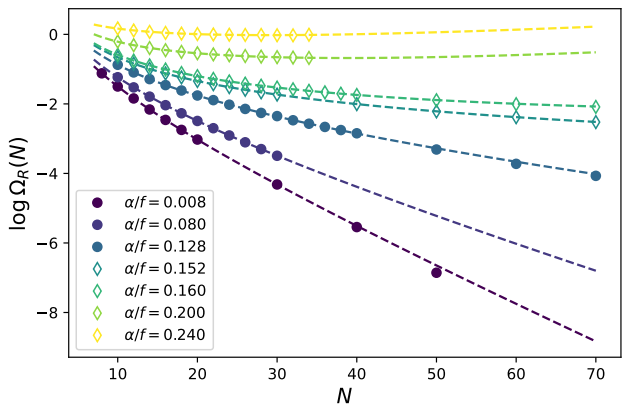


FIG. 2: Evolution of order and MQT in the quantum Ising chain from weak to strong driving, simulated with TEBD, with transverse field $\kappa=0.9$. Left: antipodal magnetic order parameter – note the saturation of order at large separation for weak and strong driving regime, with apparent decay inbetween. Drive parameters for which simulations predict magnetic order is asymptotically zero (constant) are plotted with hollow diamonds (solid circles). Right: exponential decay of the Rabi freq. associated with MQT for weak drives gives way to non-exponential, nearly flat behavior vs. N as α/f increases. Drive parameters for which the best fit is exponential decay are plotted with solid circles; hollow diamonds indicate polynomial decay or constant Ω_R .

 $\alpha/f = \alpha_s/f_s$, and therefore remain constant in N. This log-over-log limit hits an empirical sweet spot where the driving frequency increases very gradually, but the system can evolve for polynomially long times before meaningfully heating. For additional recent insights into different scaling limits, mostly focusing on steady states, see Ref. [34]. We similarly choose smooth ramp profiles to minimize heating. We note finally that we cannot measure heating during evolution as we do not compute the eigenstates of the AC-dressed system, and thus can only measure it after the transverse terms are ramped down. Since the system is closed, a final measurement is sufficient to detect if the system left the ground state manifold (Fig. 1, right). Throughout this work heating was monitored vigilantly and eliminated through a combination of measures described in this paragraph.

The key results of our simulations are shown in Figs. 2-4. We first observe that one and two dimensions (and, presumably, higher dimensions) are phenomenologically identical. In all cases, we identify three distinct regimes as seen in the figures:

- (i) The weak driving regime $(\alpha/f \lesssim 0.2)$: in this limit $\Omega_R \propto N^{-c} \exp{(-\Upsilon N)}$. The scaling exponent Υ is reduced by the AC drive but the splitting still scales exponentially. At long distances $\langle Z_i Z_j \rangle$ approaches a non-zero constant, see Fig. 2. This is the same qualitative behavior as the DC (undriven) problem, and also provides a test case for quality control of our two main simulation methods.
- (ii) The crossover regime (0.2 $\lesssim \alpha/f \lesssim$ 0.3): as α/f increases, the decay exponent Υ smoothly vanishes and the tunneling time crosses over to polynomial. The value of α_s where $\Upsilon \to 0$ depends on the transverse field κ and

system geometry. In this regime $\langle Z_i Z_j \rangle$ decays slowly with distance; in 1d (Fig. 2) it appears to asymptotically approach zero, suggesting the melting of the ferromagnetic order at a phase transition. In 2d the large-distance behavior of the order parameter is less clear, limited by the comparatively small system sizes accessible in simulation, a question NISQ computing can resolve.

(iii) The strong driving regime $(\alpha/f \gtrsim 0.3)$: $\langle Z_i Z_j \rangle$ begins to increase and becomes constant as a function of distance. Ω_R likewise becomes approximately constant with system size, though the total time required to tunnel between states is polynomial because a polynomially long ramp time is required to avoid heating.

The strong driving regime here is particularly surprising. As α increases, we observe this behavior regime begins close to $\alpha/f \sim 0.3$ in both studied dimensions and, importantly, for a variety of κ values, in contrast to regimes (i) and (ii) which are much more sensitive to κ/J . Our approximate analytic calculation is able to capture the variation of Rabi frequency in the weak drive regime (i) and also the onset of (ii) in a modified version of Eq. (2) (see SM), this derivation does not capture the restoration of order at strong driving, even with accurately extracted (numerically) Floquet Hamiltonian (see SM), thus presenting an open problem which likely requires a more nuanced treatment of non-equilibrium and non-perturbative effects.

We can further explore the non-equilibrium nature of the strong driving regime by examining the temporal evolution of the same antipodal correlator we used to define long range order in 1d. The existence of paramagnetic intermediate α regime is probed during the ramp, as the magnetic order appears to nearly collapse but then revive

briskly in time for the plateau, see Fig. 4. As mentioned above, the Rabi oscillation rate Ω_R measured from varying the plateau time is approximately constant with system size. Ω_R in this limit is a continuous function of κ , α and f and not a simple multiple of any of them. This is in stark contrast to simply using a large DC transverse field (e.g. $\kappa > \kappa_c$), where no such order restoration is seen and magnetic order decays exponentially with N in the plateau region. However, the ramping time to reach the plateau without heating the system does increase with N, empirically as $O(N^2)$ in 1d, which combined with the decreasing minimum ferromagnetic order parameter (during the ramp) suggests to us that we cross at least one, possibly two, phase transitions en route to the ferromagnetic state at strong drive. Taken together with the vastly more complicated temporal dynamics of this correlator on the plateau, which shows strong high frequency components averaged over and not shown in the Fig. 4, and the inability of the quasi-equilibrium average Hamiltonian approach (see SM) to capture the restoration of order parameter, our numerical results suggest the importance of non-equilibrium effects, such as prethermalization.

A natural and obvious extension of the results of this Letter is accelerated quantum optimization, though we caution that the spin glass case is much more complex (for example, no longer being a simple ferromagnet, the pair-flip terms generated will no longer be sign-definite and can interfere destructively with the DC transverse field). Applying a simple uniform AC field everywhere

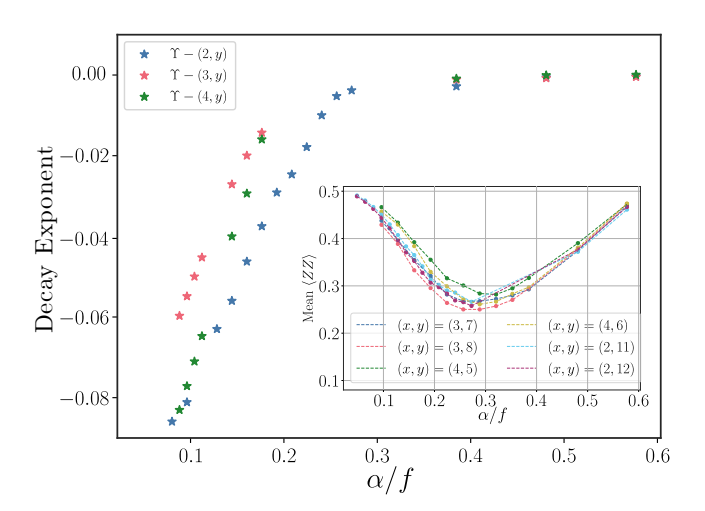


FIG. 3: Collapse of exponential slowdowns with strong drives in 2d, for various geometries with $12 \leq N \leq 28$, with the time-averaged magnetic order parameter plotted in the inset for four relatively large system sizes. As the decay exponent $\Upsilon \to 0$, the polynomial prefactor in Ω_R reduces to nearly constant scaling in the very strong drive limit. We used a transverse field $\kappa = 2.5$ for $3 \times y$ and $4 \times y$ geometries, and 1.75 for $2 \times y$.

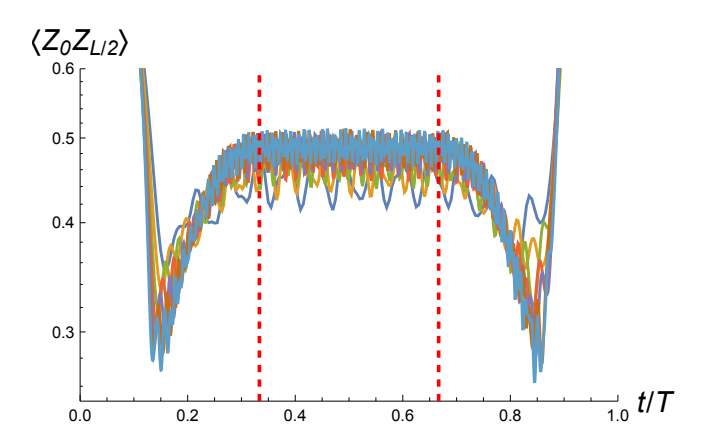


FIG. 4: Time-averaged magnetic order as probed with antipodal correlator in 1d chains of length 8 to 20 (dark blue, gold, green, red, purple, brown, light blue) at strong AC drive. Red dashed lines demarcate waiting time in-between the on-/off-ramp whereby both DC and AC transverse fields are simultaneously turned on. Contrary to conventional behavior the order parameter achieves its minimal value *during* the ramp and then recovers rather dramatically on the plateaus.

is not expected to produce significant benefits for such problems, necessitating a more sophisticated approach. That said, it may be helpful in mitigating some of the slowdowns associated with minor embedding [7] in analog quantum optimization, by inducing fast MQT in the chains that embed logical qubits in 2d systems.

Another natural next step would be to test these predictions on real quantum hardware. The feasibility of such an experiment is bolstered by the recent Quantum Utility experiment of the IBM team [35], which demonstrated accurate simulation of time evolution in a TFIM with up to 127 qubits, by combining multiple error mitigation techniques. Our discoveries here present a concrete, physically relevant, test: Floquet engineering of fast MQT coexisting with broken symmetry. The apparent universality of our results strongly suggests that this phenomenon is real at large scales in higher dimensions, but one of course needs to do an experiment on quantum computing hardware to be certain. The oscillation periods in the strong drive regimes in Figs. 2 and 3 are empirically quite short, in the range of 10-20 Trotter steps. We estimate that with a bit more effort put into fine tuning the ramping profile, system parameters, and circuit, perhaps using novel methods such as [36], present or near-term quantum hardware could simultaneously extract the scaling of the oscillation period and ferromagnetic order parameter for a hundred or more qubits. This would be one of the first uses of a quantum computer to answer a question of genuine scientific interest at beyond-classical scales, a significant milestone in the progress of quantum information science.

In conclusion, using a mix of theoretical arguments and large scale numerical simulations, with the transverse field Ising ferromagnet as a model system, we have shown that strong, high frequency AC drives can dramatically increase macroscopic quantum tunneling rates, inducing a crossover from exponential to polynomial or even constant scaling with system size. We further observed an unusual but consistent *increase* in the time averaged magnetic order with very strong driving, coexisting with fast MQT. This new dynamical phase is not explained by our analytical theory and deserves further analysis. As large MQT events form a key bottleneck in quantum algorithms, novel methods to accelerate them based on extensions of this work could have broad impact.

We would like to thank Tom Iadecola, Peter Orth, Anatoli Polkovnikov and especially Marin Bukov for useful discussions. We would also like to thank Takuto Komatsuki and Joey Liu for support with HPC calculations. This work was supported in part by the DARPA Reversible Quantum Machine Learning and Simulation program under contract HR00112190068, as well as by National Science Foundation grants PHY-1653820, PHY-2210566, DGE-2125899. G.G. was additionally supported by ARO grant No. W911NF-18-1-0125. E.K's advisory role in the project, and G.G's quantum simulations, were supported by the U.S. Department of Energy, Office of Science, National Quantum Information Science Research Centers, Superconducting Quantum Materials and Systems Center (SQMS) under contract number DE-AC02-07CH11359, with G.M.'s work funded under the NASA-DOE interagency agreement SAA2-403602 governing NASA's work as part of the SQMS center. G.M. is a KBR employee working under the Prime Contract No. 80ARC020D0010 with the NASA Ames Research Center, and additionally acknowledges support from DARPA under IAA 8839, Annex 128. Resources supporting this work were also provided by the NASA High-End Computing (HEC) Program through the NASA Advanced Supercomputing (NAS) Division at the Ames Research Center. Many of the numerical simulations in this work were performed with a generous grant of HPC access from the Fujitsu Corporation. Part of this research was performed while the one of the authors was visiting the Institute for Pure and Applied Mathematics (IPAM), which is supported by the National Science Foundation (Grant No. DMS-1925919). The Flatiron Institute is a division of the Simons Foundation.

- * Electronic address: ekapit@mines.edu
- [1] R. W. Gurney and E. U. Condon, Physical Review 33, 127 (1929).
- [2] F. Hund, z. Phys 43, 805 (1927).
- [3] L. Esaki, Physical review **109**, 603 (1958).
- [4] X. Zhao, D. A. Alcala, M. A. McLain, K. Maeda, S. Potnis, R. Ramos, A. M. Steinberg, and L. D. Carr, Physical

- Review A 96, 063601 (2017).
- [5] H. J. Lipkin, N. Meshkov, and A. Glick, Nuclear Physics 62, 188 (1965).
- [6] P. W. Anderson, Science **177**, 393 (1972).
- [7] G. Mossi, V. Oganesyan, and E. Kapit, arXiv preprint arXiv:2306.10632 (2023).
- [8] C. Weiss and Y. Castin, Journal of Physics A: Mathematical and Theoretical 45, 455306 (2012).
- [9] Y. Shin, M. Saba, A. Schirotzek, T. Pasquini, A. Leanhardt, D. Pritchard, and W. Ketterle, Physical Review Letters 92, 150401 (2004).
- [10] S. Potnis, R. Ramos, K. Maeda, L. D. Carr, and A. M. Steinberg, Physical review letters 118, 060402 (2017).
- [11] P. Cristofolini, G. Christmann, S. I. Tsintzos, G. Deligeorgis, G. Konstantinidis, Z. Hatzopoulos, P. G. Savvidis, and J. J. Baumberg, Science 336, 704 (2012).
- [12] I. Carusotto and C. Ciuti, Reviews of Modern Physics 85, 299 (2013).
- [13] M. Grifoni and P. Hänggi, Physics Reports 304, 229 (1998).
- [14] A. Eckardt, Reviews of Modern Physics 89, 011004 (2017).
- [15] M. Arndt, O. Nairz, J. Vos-Andreae, C. Keller, G. Van der Zouw, and A. Zeilinger, nature 401, 680 (1999).
- [16] S. Nimmrichter and K. Hornberger, Physical review letters 110, 160403 (2013).
- [17] F. Serwane, G. Zürn, T. Lompe, T. Ottenstein, A. Wenz, and S. Jochim, Science 332, 336 (2011).
- [18] E. Farhi, J. Goldstone, and S. Gutmann, arXiv preprint arXiv:1411.4028 (2014).
- [19] T. Albash and D. A. Lidar, Reviews of Modern Physics 90, 015002 (2018).
- [20] B. Altshuler, H. Krovi, and J. Roland, Proceedings of the National Academy of Sciences 107, 12446 (2010).
- [21] S. Knysh, Nature communications 7 (2016).
- [22] Z. Tang and E. Kapit, Physical Review A 103, 032612 (2021).
- [23] E. Kapit and V. Oganesyan, Quantum Science and Technology 6, 025013 (2021).
- [24] T. Oka and S. Kitamura, Annual Review of Condensed Matter Physics 10, 387 (2019).
- [25] H. F. Trotter, Proceedings of the American Mathematical Society 10, 545 (1959).
- [26] M. Schmitt, M. M. Rams, J. Dziarmaga, M. Heyl, and W. H. Zurek, Science Advances 8, eabl6850 (2022).
- [27] D. A. Abanin, W. De Roeck, and F. Huveneers, Physical review letters 115, 256803 (2015).
- [28] K. Mallayya and M. Rigol, Physical review letters 123, 240603 (2019).
- [29] D. V. Else, W. W. Ho, and P. T. Dumitrescu, Physical Review X 10, 021032 (2020).
- [30] F. Machado, D. V. Else, G. D. Kahanamoku-Meyer, C. Nayak, and N. Y. Yao, Physical Review X 10, 011043 (2020).
- [31] H. Zhao, F. Mintert, R. Moessner, and J. Knolle, Physical Review Letters 126, 040601 (2021).
- [32] C. Shkedrov, M. Menashes, G. Ness, A. Vainbaum, E. Altman, and Y. Sagi, Physical Review X 12, 011041 (2022).
- [33] T. N. Ikeda, S. Sugiura, and A. Polkovnikov, arXiv preprint arXiv:2311.16217 (2023).
- [34] A. Morningstar, D. A. Huse, and V. Khemani, Phys. Rev. B 108, 174303 (2023), URL https://link.aps.

- org/doi/10.1103/PhysRevB.108.174303.
- [35] Y. Kim, A. Eddins, S. Anand, K. X. Wei, E. Van Den Berg, S. Rosenblatt, H. Nayfeh, Y. Wu, M. Zaletel, K. Temme, et al., Nature **618**, 500 (2023).
- [36] T. Eckstein, R. Mansuroglu, P. Czarnik, J.-X. Zhu, M. J. Hartmann, L. Cincio, A. T. Sornborger, and Z. Holmes, arXiv preprint arXiv:2303.02209 (2023).

Supplemental material: Exponential acceleration of macroscopic quantum tunneling in a Floquet Ising model

George Grattan^{1,2}, Brandon A. Barton^{1,3}, Sean Feeney¹, Gianni Mossi^{5,6}, Pratik Patnaik^{1,4},

Jacob C. Sagal¹, Lincoln D. Carr^{1,3,4}, Vadim Oganesyan^{7,8,9}, and Eliot Kapit^{1,4*}

¹ Quantum Engineering Program, Colorado School of Mines, 1523 Illinois St, Golden CO 80401

² Department of Computer Science, Colorado School of Mines, 1500 Illinois St, Golden CO 80401

³ Department of Applied Mathematics and Statistics,

Colorado School of Mines, 1500 Illinois St, Golden CO 80401

⁴ Department of Physics, Colorado School of Mines, 1523 Illinois St, Golden CO 80401

⁵ KBR, Inc., 601 Jefferson St., Houston, TX 77002, USA.

⁶ Quantum Artificial Intelligence Lab. (QuAIL),

NASA Ames Research Center, Moffett Field, CA 94035, USA.

⁷ Department of Physics and Astronomy, College of Staten Island, CUNY, Staten Island, NY 10314, USA

⁸ Physics program and Initiative for the Theoretical Sciences,

The Graduate Center, CUNY, New York, NY 10016, USA and

⁹ Center for Computational Quantum Physics, Flatiron Institute, 162 5th Avenue, New York, NY 10010, USA*

A. Simulation details

We now present some more precise details of our simulations. Unless otherwise noted, we used a ramp time $T_r = N/8$ with a smooth sinusoidal protocol. To avoid edge effects, we used periodic boundary conditions in all cases. During evolution we measured the ferromagnetic order parameter $\langle Z_i Z_j \rangle$ between the two most distant qubits, to characterize the instantaneous state of the system. This quantity was time-averaged over the plateau to eliminate high frequency modulations. To simulate evolution under a high frequency AC drive, we chose a decreasing timestep dt = c/f sufficiently small to appropriately sample it. dt too large leads to severe Trotter error and nonsensical output; c between 0.15 and 0.4 was sufficient for faithful simulations, with smaller values necessary when α is large. Our results thus simulate continuous time and are not due to time discretization. The Trotter error was eliminated by choosing an appropriate timestep dt = c/f with value of c between 0.25 and 0.125. The bond dimension χ values in our 1d TEBD simulations was chosen up to 50.

For a given system size N and α/f value, the Rabi frequency Ω_R is estimated by simulating the Floquet protocol for times t_1, t_2, \ldots, t_n obtaining the tunnelling probabilities p_1, p_2, \ldots, p_n , where $p_i \equiv |\langle 1 \cdots 1 | U(t_i) | 0 \cdots 0 \rangle|^2$. Ω_R is then extracted by fitting the data with the function $p(t) = \sin^2(\Omega_R t + \phi_{init})$, as shown in Fig. 1(right panel). For all simulations, the ramptimes and plateau times were chosen so that (i) heating observed would introduce only negligible effects in the extracted value of the Rabi frequency, and (ii) the probed times would allow us to follow at least one oscillation of the tunnelling probability.

When fitting the data, we used a Fast Fourier Transform on the state population data to obtain a warm start for the frequency. Additionally we fit the Rabi frequency for both $|\langle \psi(T)|1\rangle|^2$ and $|\langle \psi(T)|0\rangle|^2$ and the reported value is the mean of these two values. There were in-

stances where we needed to add a phase of $\pi/2$ to ϕ_{init} in order to help the model to fit the data, this is likely due to the size dependent simulation times, which caused inconsistent "initial" populations/ initial phases. Additionally in instances with a heating we used a model that included a decaying exponent term, namely p(t) = $e^{-bt}\sin^2(\Omega_R t + \phi_{init})$ and we found little inconsistency in the extracted values for Ω_R in these cases. We then logarithmically scaled the values of Ω_R , as seen in Supplementary Figure 1 and fit them to $\log(\Omega_R) = A + \Upsilon * N$ in order to extract the difficulty exponent Υ seen in 3.In 1d our fits were to $\log(\Omega_R) = A + B \log N + \Upsilon * N$, as the larger system sizes accessible through TEBD allowed us to resolve polynomial prefactors more accurately. In both cases we observe that the Rabi frequency decays exponentially with the system size at small values of α/f and enters a "fast tunnelling" regime at larger values. In the 1d case small positive values of the difficulty exponent Υ (see Fig. 2) are observed in the fast tunnelling regime while Ω_R is still slowly decaying with the system size. We believe these to be an artifact of the fit due to finite size, and interpret them to be compatible with $\Upsilon = 0.$

B. Theory of MQT in the 1d TFIM

We consider the 1d transverse field Ising model, in the ferromagnetic phase. Our Hamiltonian is

$$H = -\sum_{j} \left(\kappa X_j + J Z_j Z_{j+1} \right) \tag{1}$$

We assume periodic boundary conditions, for simplicity. Our goal is to compute the exponentially small tunneling rate Ω_0 between degenerate ground states in the ferromagnetic phase, where $\kappa < J$, through Lth order perturbation theory in κ using the Ising Hamiltonian as the base Hamiltonian. Fundamentally, this is a sum of L! flip sequences connecting the two classical ground

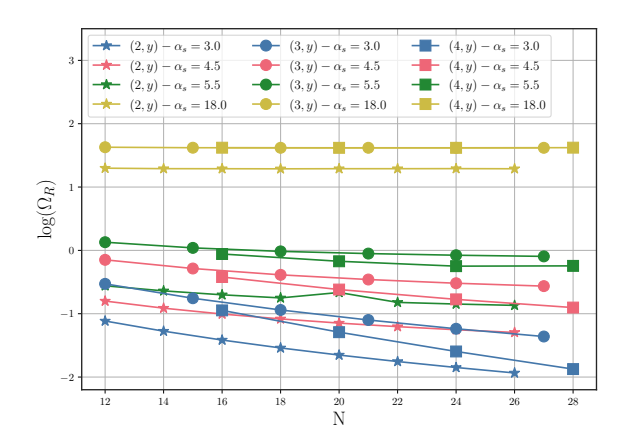


FIG. 1: Lograthmically scaled Rabi oscillations in the twodimensional transverse-field model, with $\kappa=2.5$. Collections of data such as this one are used to extract the difficulty scaling exponent and characterize the three drive strength regimes.

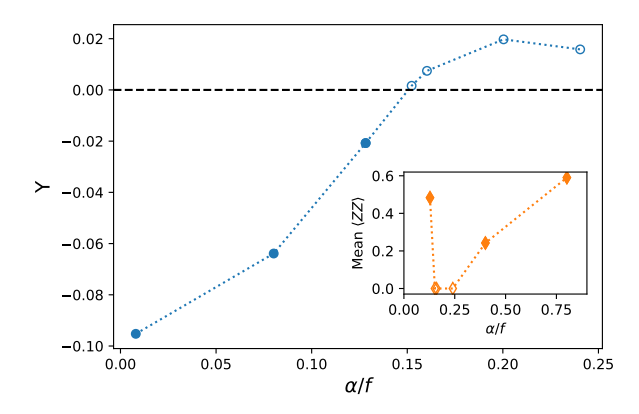


FIG. 2: Difficulty exponents Υ extracted from Fig. 2.Solid dots indicate datapoints where Ω_R decays exponentially, while empty circles are compatible with subexponential decay. Inset: time-averaged values for the two-point correlator from Fig. 2.Filled diamonds indicate values of α/f where we observe saturation of $\langle Z_0 Z_{L/2} \rangle$ in the range of system sizes observed. Empty diamonds label cases where no such saturation is observed, which we conservatively interpret a zero magnetization.

states??????, e.g.

$$\Omega_0 \simeq \kappa^L \sum_{perm.seq\{s_j\}} \prod_{k=1}^L \frac{1}{E_{\{s_1, s_2 \dots s_k\}}}$$
 (2)

Now, with L! terms and strong path dependence in the denominator, this expression looks hopeless. But it turns out there are two limits where one can evaluate sums of this form, to good approximation. One is infinitedimensional (e.g. random) graphs or hypergraphs, where the influence of specific sequences with (comparatively) low intermediate energies, which have higher weight in the sum, is swamped by the combinatorical proliferation of random sequences, an issue we take up in a forth-coming publication. The other is limit is 1d, e.g. this problem. It will become clear from the structure of the derivation why 2d is considerably harder and we do not attempt it here.

The trick to evaluating this sum is to organize the sets of terms by the maximum number of domain wall pairs created at intermediate steps. We'll start with the simplest process, where there is just a single pair of domain walls at all steps. This process begins by enacting a single flip at any of the L sites, which has an energy cost 4J. The next flip is at one of the two sites adjacent to this, which moves one of the two domain walls further apart by one step. The intermediate energy is still 4J, but there are two choices we can make, which gives us a combinatorical factor of 2 in the numerator. The same goes for the third flip, fourth flip, and so on, "unzipping" down the chain and accumulating a factor of $\kappa/2J$ at each step. Noting that there were L choices for the first site to flip.

$$\Omega_0^{(1)} = L \frac{\kappa^2}{4J} \left(\frac{\kappa}{2J}\right)^{L-2} = L \frac{\kappa}{2} \left(\frac{\kappa}{2J}\right)^{L-1} \tag{3}$$

This is the lowest energy path possible, so one would be tempted to stop here. But doing so underestimates Ω_0 by a factor of 2^L , which isn't great. To get the correct value—or at least, the correct exponent—we need to consider higher order terms.

Let's now consider the set of all processes where a second pair of domain walls is is created at some intermediate stage. Assume that k = 1 is the first step and the first k flips simply create the first pair and separate them. Then we now have a total of (L-k-2) choices for where to nucleate the second pair (the -2 comes from two sites just moving existing domain walls around), and the energy cost once this is done is 8J (compared to 1/2J, counting the combinatorics, for a flip at this stage that just moves a domain wall). This is the energy cost that now shows up in the dominator at each subsequent order until a pair of domain walls eventually fuses, but we now have 4 sites we can flip to move a domain wall around, so we get a factor of $\kappa/2J$ at each subsequent step just like if we had a single pair, and once one of the pairs is eliminated we're back to the same result as above. Combining all these factors, and summing over space and "time" points where the second pair is created, we get:

$$\Omega_0^{(2)} \simeq \sum_{k=1}^{L-2} \frac{L-k-2}{4} \Omega_0^{(1)}.$$
(4)

Now with three intermediate pairs. The third pair is nucleated at any step after k, called step l. At this step there are (L-l-4) sites to choose from, and the energy cost is 12J (corresponding to a factor of 1/6 in comparison to a flip that just moves a domain wall). Noting the factor of 1/4 from the previous sequence, and ignoring the combinatorically subleading cases where the second

pair of domain walls was destroyed before this third pair was created, we find

$$\Omega_0^{(3)} \simeq \sum_{k=1}^{L-2} \frac{L-k-2}{4} \sum_{l=k}^{L-4} \frac{L-l-4}{6} \Omega_0^{(1)}.$$
 (5)

We can generalize this to four intermediate pairs, by inspection:

$$\Omega_0^{(4)} \simeq \sum_{k=1}^{L-2} \frac{L-k-2}{4} \sum_{l=k}^{L-4} \frac{L-l-4}{6} \sum_{m=l}^{L-4} \frac{L-m-6}{8} \Omega_0^{(1)}.(6)$$

If we evaluate these sums in mathematica, a pattern quickly emerges, and a bit of algebra and inspection shows that at order p we have

$$\Omega_0^{(p)} \simeq \left[\frac{p}{2^{2p-1} (p!)^2} \prod_{k=2}^{2p-1} (L-k) \right] \Omega_0^{(1)}.$$
(7)

The product evaluates to a Pochhammer function. Our total tunneling rate is given by taking this sum out to L/2, the maximum number of domain wall pairs possible in this system:

$$\Omega_0 \simeq L \frac{\kappa}{2} \left(\frac{\kappa}{2J}\right)^{L-1} \sum_{p=1}^{L/2} \left[\frac{p}{2^{2p-1} (p!)^2} \prod_{k=2}^{2p-1} (L-k) \right].$$
 (8)

This is a sum Mathematica can do; we get

$$\Omega_0 \simeq \frac{L}{4} \kappa \left(\frac{\kappa}{J}\right)^{L-1} \frac{\Gamma(L-1/2)}{\sqrt{\pi}L!}$$
(9)

Aymptotically, the ratio $\Gamma(L-1/2)/L!$ converges to $L^{-3/2}$, so up to an overall constant prefactor

$$\Omega_0 \propto \frac{\kappa}{\sqrt{L}} \left(\frac{\kappa}{J}\right)^{L-1}.$$
(10)

This matches numerics extremely well, though numerical data suggests a polynomial prefactor of $L^{-\kappa/J}$ is a slightly better fit. That the exponent is such a close match is a real triumph for high order perturbation theory.

C. Average Hamiltonian

Standard Floquet-Magnus perturbation theory may be used to compute the average Hamiltonian in the regime of weak drive α . Recall Eq. 1with $\kappa = 0$, for now

$$H(t) = -J \sum_{\langle ij \rangle} Z_i Z_j + \alpha \sin \omega t \sum_i Y_i \to H_0 + \delta H(t) (11)$$

The leading nontrivial contribution to the average Hamiltonian comes from the third order in the Magnus expan-

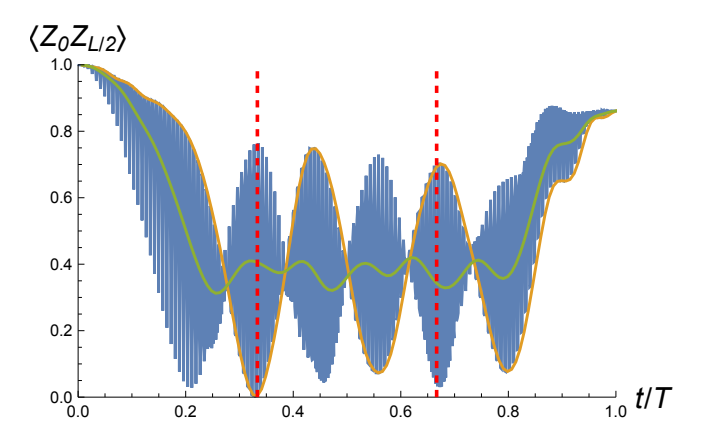


FIG. 3: Sampling dependence of $\langle Z_0 Z_{L/2} \rangle$ in the strongly driven regime. The blue trace samples it at every timestep, gold at the end of every full period (dt=1/(5f) here), and green sampling at every timestep but reporting the average over each full period. The strong discrepancy between the gold and green curves suggests that the fast MQT ferromagnetic state is not a simple doublet of the two lowest quasienergy states of the Floquet unitary. See text for detailed simulation parameters. Red dashed lines demarcate the plateau region.

sion

$$H^{(3)} = \frac{1}{6} \int_{0}^{t} dt_{1} \int_{0}^{t_{1}} dt_{2} \int_{0}^{t_{2}} dt_{3}([H(t_{1}), [H(t_{2}), H(t_{3})] + [H(t_{3}), [H(t_{2}), H(t_{1})] \rightarrow J\left(\frac{\alpha}{f}\right)^{2} \sum_{j} (\mathbf{Z}_{j}\mathbf{Z}_{j+1} - \mathbf{X}_{j}\mathbf{X}_{j+1}),$$
(12)

which both suppresses magnetic ZZ interactions and promotes domain wall creation and hopping, in pairs (the use of f rather than ω respects our convention of including a factor of 2π in time evolution). Single domain wall terms at finite κ are expected to renormalize approximately as $\kappa \to \kappa(\alpha) \approx J_0(2\alpha/f)$. To complement and extend these analytic results we may compute the average hamiltonian of small lattices for arbitrary couplings by first computing the (numerically exact, for a fixed dt) unitary evolution operator, then inferring the average hamiltonian from its numerical matrix logarithm and then, finally, decomposing it into Pauli strings. This procedure appears extremely stable against system size variations as it results in rather short-ranged average Hamiltonians, with trace-norm of the operator saturated to better than fraction of a percent with one- and two-site terms. As expected, we observe the expected suppression of the static ZZ and X interactions and the growth of XX interactions. We also observe the unexpected nonmonotonic growth and then decay of single spin Y terms which may be responsible for the demise of magnetic order at intermediate values of α we observe both in 1d and 2d dynamics. Importantly, direct exact diagonalization of the average Hamiltonian for its ground state and low lying states over

a range of system sizes corroborates the observed variation of the Rabi frequency with system size in both weak and strong driving regimes. This direct approach does not reproduce the observed restoration of ZZ correlator.

D. Collective tunneling in the AC driven case

In the weak and crossover regimes, the average Hamiltonian formulation predicts both the renormalization of κ and J from fast oscillations, and the generation of new pair-flip terms that constructively interfere to accelerate tunneling. We can incorporate all these effects into the derivation of Eq. 10 to predict both the reduction of the scaling exponent Υ in the weak driving regime, and the approximate location of the crossover to polynomial scaling by identifying where $\Upsilon \to 0$. The renormalization of κ and J is straightforward–following the arguments in?, κ is reduced by a factor of $J_0(2\alpha/f)$, where J_0 is a Bessel function. Note that the argument is α/f and not α/ω , respecting the convention stated in the main text of including a factor of 2π in front of H(t) in time evolution. Since the ferromagnetic coupling J involves two-spin terms it is reduced by a factor of $J_0(2\alpha/f)^2$, at least in the limit of α/f small, and thus the ratio κ/J is increased by a factor of $1/J_0(2\alpha/f)$.

To incorporate the pair flip terms, we need to take into account two sets of processes. The first moving a domain wall by two steps, with matrix element $-J\frac{\alpha^2}{f^2}$ (as compared to moving it a single step with matrix $-\kappa$ in the DC transverse field), and creating a domain wall pair two sites apart with matrix element $-J\frac{\alpha^2}{f^2}$. The energy denominators depend on the Ising Hamiltonian and are thus unchanged beyond the renormalization of J already discussed. We can incorporate these terms into the analysis leading to 10, at least approximately, by making two substitutions. First, noting that "most" of the spin flips that contribute to the tunneling amplitude consist of moving domain walls, we can now replace any single flip (which contributes $\kappa/(2J)$ when all combinatorics are considered) with a pair flip with amplitude $2\frac{\alpha^2}{f^2}$ (including 1/Jfor the energy denominator). This replaces two orders in the DC calculation, and so the combination of all such processes multiplies the tunneling rate by $\left(1+2\frac{\alpha^2J^2}{f^2\kappa^2}\right)^L$, to decent approximation. The second modification is that every step that nucleates a new domain wall pair can be replaced by the corresponding process that creates such a pair two flips apart, which removes a factor of $\kappa/(4J)$ from the overall tunneling rate since it flips two spins instead of one. Combining all these contributions, we derive an AC-modified tunnel splitting

$$\Omega_{R}(\kappa, \alpha, f, L) \simeq L \frac{\kappa}{2} \left(\frac{\kappa}{2J \times J_{0} \left(2\frac{\alpha}{f} \right)} \right)^{L-1} \times (13)$$

$$\left(1 + 2\frac{\alpha^{2}J^{2}}{f^{2}\kappa^{2}} \right)^{L} \times \sum_{p=1}^{L/2} \left[\frac{p \left(1 + 4\frac{\alpha^{2}J^{2}}{f^{2}\kappa^{2}} \right)^{p}}{2^{2p-1} \left(p! \right)^{2}} \prod_{k=2}^{2p-1} (L - k) \right].$$

This expression must be evaluated numerically, but it's straightforward to do so. The decay exponent decreases continuously with α/f , and if this ratio becomes large enough the decay exponent crosses zero. At this point perturbation theory has broken down and we expect a crossover to polynomial decay (as observed in our simulations), though we cannot predict the degree of that polynomial with these methods. For $\kappa=0.9$, Eq. 13 predicts $\Upsilon\to 0$ when $\alpha/f\simeq 0.15$, in excellent agreement with the simulations shown in Fig. 2.

E. Breakdown of the average Hamiltonian approach in the strong driving regime

This treatment, while effective for predicting the system's behavior in the weak driving and crossover regimes, is not sufficient to capture all the interesting physics in the strong driving regime, where magnetization revives (see FIG. 4 for a particularly dramatic illustration of this effect). Beyond the fact that nothing in the strengthening of transverse terms (and more rapid weakening of J relative to κ) predicts a magnetic order restoration, an additional clue can be seen in the detailed time dynamics of the magnetic order $\langle Z_0 Z_{L/2} \rangle$ in 1d, as shown in FIG. 3. In that plot, we simulated a 1d ring with N=10, $t_r=N^2/64$, plateau time $N^2/64$, $\kappa=0.5$, $f_s=12$, $\alpha_s=5.8$, and dt=1/(5f). AC and DC transverse fields are ramped up and down with the same profile. There is nothing special about these specific parameters and the behavior we now describe is general for strong driving.

As seen in the figure, different choices of how to sample $\langle Z_0 Z_{L/2} \rangle$ produce very different results, particularly in the comparison of sampling at the end of each Floquet period with reporting the average over each Floquet period. As described earlier, in all low-heating cases the system displays clean and coherent Rabi oscillation dynamics when varying the plateau time and measuring the populations of $|000...\rangle$ and $|111...\rangle$ at the end of the ramp. It is tempting to assume from this that in the plateau the dynamics is captured by oscillations within a simple doublet of the two lowest quasienergy states of the Floquet unitary, in analogy to the DC case with $\kappa < \kappa_c$. And while this picture is good for weak driving, in the strong regime the observed large discrepancy between the magnetic order measured at the end of each Floquet period (which exhibits very large oscillations) and the same quantity averaged over each full

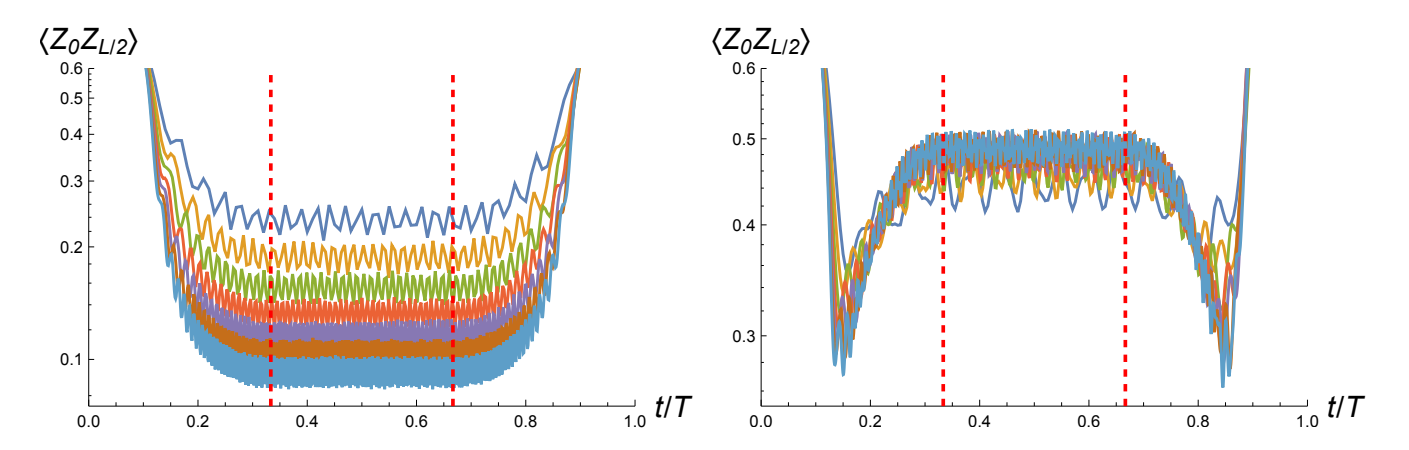


FIG. 4: Comparison of the time-averaged magnetic order parameter for large DC transverse field (a) and strong AC drives (b), measured over the full evolution time, in the 1d chain with L running from 8 to 20 in steps of 2. Red dashed lines demarcate waiting time in between the ramps. In the DC case on the left, κ is ramped up to 2, well past $\kappa_c = 1$, and the residual magnetic order decays exponentially with L as a result. In the AC case on the right, κ is ramped up to 0.9 and the AC field is ramped into the strong driving regime with $\alpha_s = 7.7$ and $f_s = 12$. Here the long-range magnetic order is constant with system size in the plateau, but as the fields are ramped up, it does cross a minimum value which is slowly decreasing with L, suggesting a phase transition is crossed. $\langle Z_0 Z_{L/2} \rangle$ begins and ends at 1 (when all transverse fields are turned off) but this region is left off the plot to better focus on the behavior in the ramping and plateau regions.

cycle (which exhibits small oscillations around an average value) suggests that the dynamics in this regime are significantly more complex. A more sophisticated, likely

at least partially nonperturbative, analysis could shed light on the detailed properties of this unusual state.

^{*} Electronic address: ekapit@mines.edu